











Search for possible fission modes at high excitation energies in ^{254}Fm

Tathagata Banerjee ^{1,*}, E. M. Kozulin ^{1,2}, N. T. Burtebayev ², K. B. Gikal ¹, G. N. Knyazheva ¹, I. M. Itkis ^{1,2},
K. V. Novikov ¹, T. N. Kvochkina ², Y. S. Mukhamejanov ^{1,2} and A. N. Pan ²

¹Flerov Laboratory of Nuclear Reactions, Joint Institute for Nuclear Research, Dubna 141980, Russia

²Institute of Nuclear Physics of the Ministry of Energy of the Republic of Kazakhstan, Almaty 050032, Republic of Kazakhstan



(Received 23 February 2022; accepted 1 April 2022; published 19 April 2022)

Background: Shell effects have been found to influence both the compound nuclear fission (CNF) and quasifission processes. Besides quasifission processes, which fission modes remain active at excitation energy (E^*) as high as 56 MeV should be investigated.

Purpose: We investigate the signatures of fission modes in ^{254}Fm populated by $^{16}\text{O} + ^{238}\text{U}$ through the mass distribution (MD) and total kinetic energy distribution (TKED).

Method: The mass–total kinetic energy distributions (M-TKED) of fission fragments of the reaction $^{16}\text{O} + ^{238}\text{U}$ have been measured at two laboratory energies $E_{\text{lab}} = 89$ and 101 MeV. The spontaneous fission (SF) of ^{254}Fm , one-dimensional (1D) fragment MD, and two-dimensional (2D) M-TKEDs of $^{16}\text{O} + ^{238}\text{U}$ have been described by the multimodal random neck rupture (MM-RNR) model.

Results: Channel probabilities and the characteristics of different fission modes are obtained and discussed in detail. The enhancement observed in the mass yield ($\approx 10^{-2}\%$) in the region 60–70 u for the light fragments at $E^* \approx 45$ MeV goes away at the higher $E^* \approx 56$ MeV. The heavy fragments of S1 and S2 modes are found to be associated with $Z \approx 53$ and $Z \approx 56$ shells, respectively. The slope of asymmetric to symmetric fission yields (when plotted against E^*) of $^{16}\text{O} + ^{238}\text{U}$ is found to be similar to that of previously reported $^{18}\text{O} + ^{208}\text{Pb}$.

Conclusions: Analysis of 2D M-TKED data by the MM-RNR model reveals the possible presence of fission modes in $^{16}\text{O} + ^{238}\text{U}$. The liquid-drop-like broad symmetric SL mode is found to peak at a lower energy than predicted by the Viola systematic, which matches mostly with that of Standard 2 mode. No signature of asymmetric quasifission is observed. The MD widths show a linear dependence with the measured energies.

DOI: [10.1103/PhysRevC.105.044614](https://doi.org/10.1103/PhysRevC.105.044614)

I. INTRODUCTION

Two reacting nuclei after surmounting the interaction (fusion) barrier, i.e., capture, form a composite system, which can lead to several dissipative processes: fusion, quasifission [1], and fast fission [2]. A compound nucleus (CN) [3,4] is formed when two nuclei completely fuse after full momentum transfer and the composite system equilibrates in all degrees of freedom. The CN can further yield a cold evaporation residue (ER) after emitting high energy statistical γ rays, neutrons, light charged particles, and/or splits (nearly) symmetrically into two halves (compound nuclear fission = CNF) under the influence of strong Coulomb repulsion. Unlike in CNF, in quasifission, the composite system splits before moving inside the fission saddle point, either without significant mass transfer (asymmetric quasifission = AQF) or with significant mass transfer (symmetric quasifission = SQF). Quasifission occurs on a shorter timescale than fusion but longer timescale than multinucleon transfer processes (quasielastic and deep inelastic) [5,6]. The AQF is caused by the influence of proton shells with $Z = 28, 82$ and neutron shells with $N = 50$ and 126; it occurs in less than half a

rotation of the composite system (sticking time of < 10 zs), as seen in mass-angle correlation, and resides at the lower end of the total kinetic energy distribution (TKED) as the asymmetric fragments have lower TKE than the symmetric ones [7]. The SQF [8–10] occurs in a sticking time greater than that required for the system to undergo one rotation [11]. It is mainly evident from the deviation of measured fission fragment angular anisotropy (FFAA) from the (saddle-point) transition state model (TSM) [12] calculations for CNF [8,13]. It resides at the higher side of the TKED due to not having complete dissipation of the entrance channel TKE [7]. It is determined by the shells with $Z = 50$ and $N = 82$ [7]. Both the SQF and CNF can lead to the formation of symmetric fragments. Often the separation of SQF from the CNF is fraught with difficulties. While with increasing the projectile mass M_P (or charge) and consequently the increasing angular momenta brought in, the fusion barrier increases, and both the fission and quasifission barriers decrease [14]. Fast fission occurs at high angular momentum where there is no fission barrier.

A CN may also choose among various paths to disintegration upon leaving the compound state. Brosa *et al.* [15] developed a model that can decompose the mass distributions (MDs) and mass–total kinetic energy distributions (M-TKEDs) into different fission modes, namely, one

*he.tatha@gmail.com

symmetric “superlong” (SL) or “supershort” (SS) mode and four asymmetric modes: “Standard 1” (S1), “Standard 2” (S2), “Standard 3” (S3), and superasymmetric (SA). Nuclei in the region ^{225}Ra – ^{228}Ac exhibit two fission modes, namely symmetric and asymmetric, with a predominance of the asymmetric fission mode in the case of energies near the barrier [16–18]. The $\langle\text{TKE}\rangle$ of this asymmetric mode is ≈ 10 MeV higher than that of the symmetric mode. For the nuclei with mass ≈ 220 , three fission modes were observed [19]. The asymmetric component here consists of two standard modes with average masses ($\langle M_i \rangle$) of ≈ 132 and ≈ 139 with $\langle\text{TKE}\rangle$'s near ≈ 178 and ≈ 168 , respectively. In the nuclei near the line of β stability in SF or low-energy induced fission and the nuclei in the actinide region (mostly below Fm), the heavy fragments are emitted predominantly with a mass $A_H \approx 140$ [20], and the distributions can show multimodal structures [21–25]. The SF MDs of the Fm isotopes show a marked transition from asymmetric (double humped) to symmetric (single humped) as the mass number increases from 254 to 258 [26–29], along with a correlated increase in the fragment TKE by ≈ 35 MeV [30]. The transition of the asymmetric to symmetric mode has been found to be due to the fact that the symmetric mode makes a sudden transition from SL to SS fission mode around ^{254}Es , as found recently by Usang *et al.* using a four-dimensional (4D) Langevin calculation [31]. This transition from SL to SS was observed earlier by Brosa *et al.* [15]. *Thus, not only the fissioning nuclei of or near mass 254 in this transition region need special attention, but also how the probabilities of fission and quasifission processes would change in heavy ion induced fission are yet to be explored.*

Though the possibility of the fission asymmetry of the preactinides had been predicted in the 1970s [32,33], it took a decade to substantiate this prediction experimentally [34–36]. The search for SA fission has been receiving increasing interest due to its possibility of producing exotic neutron rich nuclei [37]. Recently, the superasymmetric mode due to the influence of doubly-magic Ca ($Z = 20$, $N = 28$) and doubly-magic Pb ($Z = 82$, $N = 126$) has been observed at mass yield levels of $10^{-3}\%$ and $10^{-5}\%$, in the fission of excited CN ^{260}No , populated by the reactions $^{12}\text{C} + ^{248}\text{Cm}$ and $^{22}\text{Ne} + ^{238}\text{U}$, respectively [38,39]. Lustig *et al.* [40] predicted SA fission modes in $^{253}\text{Fm}(n, f)$ and in the SF of ^{254}Fm . *Should there be any trace of such SA fission at higher excitation of ^{254}Fm populated by a heavy ion?*

The analyses of multimodal fission using both the 1D MD and 2D M-TKED in heavy ion induced reactions are scarce. The main interest of this work is searching for the possible fission modes in the reaction $^{16}\text{O} + ^{238}\text{U}$. As it populates the CN ^{254}Fm with mass 254 which falls in the aforementioned transition region, the reaction $^{16}\text{O} + ^{238}\text{U}$ makes it a nice candidate for testing. This work would then further aid in searching for quasifission modes in such reactions in future.

The experimental details are described in Sec. II. The M-TKEDs are presented in Sec. III. The possible presence of multimodal fission is investigated using the multimodal random neck rupture (MM-RNR) model [15] in Sec. IV and the widths of measured and calculated MDs are compared in Sec. V, followed by a discussion and conclusions in Sec. VI.

II. EXPERIMENTAL DETAILS

The measurements were carried out using the double-arm time-of-flight (TOF) spectrometer CORSET [41] at the Flerov Laboratory of Nuclear Reactions (Dubna, Russia). A beam of ^{16}O was used from the U400M cyclotron with $E_{\text{lab}} = 89$ and 101 MeV. The energy resolution of the beam was $\approx 1\%$. A $150 \mu\text{g}/\text{cm}^2$ thick target of ^{238}U sandwiched between $40 \mu\text{g}/\text{cm}^2$ thick carbon backing and $10 \mu\text{g}/\text{cm}^2$ thick carbon capping was used. The target was placed at the center of the reaction chamber, at an angle of 45° with respect to the beam direction. Each arm of CORSET contains a start and a position-sensitive stop detector based on microchannel plates (MCPs). The carbon foils on the start detectors were of thickness $\approx 70 \mu\text{g}/\text{cm}^2$. The start and stop detectors were placed at distances of 5 and 28.4 cm from the target, respectively. The spectrometer arms were kept at angles of $\pm 78^\circ$ with respect to the beam direction. The position resolution of the stop detectors was 0.3° . The angular acceptance of each arm was 10° in the reaction plane and 8° outside the plane. The solid angle of each spectrometer arm was ≈ 200 msr. The time resolution, determined using a ^{226}Ra alpha-particle source, was 180 ps. The uncertainty of energy losses of the fission fragments in the target, the backing material, and the converting foils of start detectors and the characteristics of the CORSET spectrometer provide the mass resolution of ≈ 2 u. The systematic error in measuring energy was estimated to be ± 5 MeV. The times of flight for both the fragments were measured, which allowed us to determine the velocities. The mass and energy values of the fragments were then determined from the measured velocities with the double-velocity method. The use of detectors based on microchannel plates (MCPs) (time resolution ≈ 180 – 200 ps) offered a good mass and energy resolution.

III. M-TKED OF FISSION FRAGMENTS OF $^{16}\text{O} + ^{238}\text{U}$

Assuming standard two-body kinematics, the experimental data were processed. With the assumption that the mass of the composite system is equal to the sum of the masses of target and projectile, the primary velocities, masses, energies, and angles in the center-of-mass frame of the reaction products were calculated from the measured velocities and angles in the laboratory frame using the momentum and mass conservation laws. Neutron evaporation before scission was not taken into account. Considering the fact that even at the highest reaction energies not more than four neutrons could be emitted and the resolution of the spectrometer being 2–3 u, the neutron emission is not expected to put visible effects on the M-TKEDs.

In reactions with such actinide targets, transfer induced fission also occurs, but at different folding angles. The binary products of the reaction were selected by putting a circular gate of radius 5° around 180° in the fission-fragment-folding-angle distributions [FFFADs] in the center-of-mass frame (reaction plane ($\theta_{c.m.}$) versus out of reaction plane ($\phi_{c.m.}$)). This contour corresponds to the momentum transfer of more than 90% [41,42] and helps to avoiding large angular deviations due to post-scission neutron emissions from the fragments which can wash out the kinematic correlations of

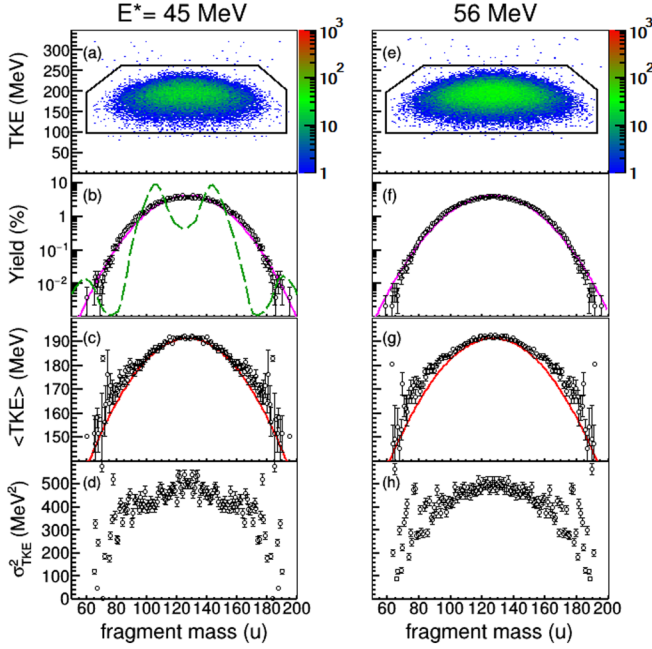


FIG. 1. M-TKEDs of the reaction $^{16}\text{O} + ^{238}\text{U}$ at two E^* 's (a) 45 MeV and (e) 56 MeV. The events inside the black gates are processed to obtain distributions in the next panels. Corresponding MDs are fitted with single Gaussians (magenta curves) of fixed width and shown in panels (b) and (f), respectively. The green dashed line in panel (b) is the theoretical calculation [40] for the reaction $^{253}\text{Fm}(n, f)$ populating the same CN ^{254}Fm . Corresponding $\langle\text{TKE}\rangle$'s are shown in panels (c) and (g) whereas the variances of the TKEDs (σ_{TKE}^2) are shown in panels (d) and (h), respectively. The continuous red curves in panels (c) and (g) represent the parabolic approximation to the symmetric component.

the complementary fission fragments. This allows a reliable determination of the M-TKEDs of binary reaction products.

M-TKEDs of the primary binary fragments obtained in the reaction under investigation at CN E^* 's of 45 and 56 MeV, MD of fission fragments, $\langle\text{TKE}\rangle$, and the variance of the TKED (σ_{TKE}^2) as functions of fragment mass are shown in Fig. 1. 2D matrices of M-TKEDs of fission fragments are presented in the upper panels [(a) and (e)] of the figure. The events within the black gate shown in those panels are processed to generate the MDs, $\langle\text{TKE}\rangle$, and σ_{TKE}^2 , which are shown in the consecutive panels.

The MDs are normalized to 200%. The experimental MDs were fitted first with single Gaussians without fixing any parameter and the obtained χ^2 's per degree of freedom of the fits were 6.83 and 6.97, respectively. Fixing the width parameters to the widths based on the liquid drop model (LDM) resulted in worsening of the fits with χ^2 's per degree of freedom 9.81 and 9.49, respectively. The continuous magenta lines are the fits after fixing the width parameter. The green dashed line in panel (b) is the theoretical calculation of static fission mass yields using a liquid-drop-model fission path and the two-center shell model by the Greiner group [40] for the reaction $^{253}\text{Fm}(n, f)$ populating the same CN ^{254}Fm at $E^* \approx 6.5$ MeV. An increase in the mass yield ($\approx 10^{-2}$ %) in the SA mass region was obtained from the calculation. In the framework

of the LDM, the $\langle\text{TKE}\rangle$ has a parabolic dependence on the fragment mass and practically does not depend on the E^* and angular momentum of the CN [43]:

$$\text{TKE}(M) = 4 \times \text{TKE}_{\text{Viola}} \frac{M(M_{\text{CN}} - M)}{M_{\text{CN}}^2}, \quad (1)$$

where M is a fragment mass and $\text{TKE}_{\text{Viola}}$ is the most probable TKE estimated using the Viola systematics [44]. As can be seen from Fig. 1, such behavior of TKE is confirmed by experimental data. The continuous red lines are parabolas with $\langle\text{TKE}\rangle$ fixed at 191.3 MeV ($\text{TKE}_{\text{Viola}}$) [44]. The deviation of the $\langle\text{TKE}\rangle$ data from the LDM expectation can be seen in the asymmetric mass regions (e.g., heavy mass range 160–190). The curve σ_{TKE}^2 has humps in the symmetric region as well as in the asymmetric regions (e.g., heavy mass range 160–190) which confirms the co-existence of several other channels in these regions. These point towards the presence of other modes and call for a multicomponent analysis indicating the effects of shell closures.

To know whether this reaction has pure CNF with multimodal structures or a combination of CNF and quasifission (AQF and/or SQF), first the presence of multimodal fission was investigated, followed by an attempt to look for quasifission.

IV. SEARCH FOR THE MULTIMODAL FISSION IN $^{16}\text{O} + ^{238}\text{U}$

Characteristics of independent fission modes are generally derived from the multicomponent analysis of fission fragment MD, TKE, or M-TKED. These can be described by the superposition of multi-Gaussians corresponding to different fission modes prescribed by Brosa *et al.* [15] (e.g., SS, SL, S1, S2, S3, and SA). The SF MD of ^{252}Cf have all these except the SS mode [15,45,46]. Though in most cases, MDs could be described by three main components (S1, S1, and S2), the S3 mode was also accommodated in some works [21,45–48] The presence of SA mode in heavy nuclei can also be found in the literature [35,38,39,49].

The SL mode is a symmetric peak, which would be situated at $\frac{M_{\text{CN}}}{2}$. It is mainly defined by the macroscopic liquid drop (LD) part of the potential energy, and only slightly distorted by shell corrections. This mode is characterized by strongly elongated scission shapes of fissioning nuclei. Both the fragments formed in the SL mode are prolate. The symmetric mode at $\frac{M_{\text{CN}}}{2}$ makes a sudden transition from SL to SS fission mode around ^{254}Es [31]. However, this SS mode becomes prominent from the mass region ≈ 258 [31,40]. Here both the fragments are oblate. If present at all, this mode would be too weak in the mass region of the present work and in such excitations [13] to change the final interpretations.

S1, S2, S3, and SA modes are asymmetric modes and would be situated on either side of the symmetric peak. The positions of these modes are determined by shell effects. The S1 mode is due to the formation of spherical heavy fragments close to proton number (Z) = 50 and neutron number (N) = 82 and mass number ((M_H)) ≈ 132 . But generally the heavy peak of this mode is situated near mass number ≈ 135 . This is usually interpreted as joining of 2–3 nucleons from a neck to a

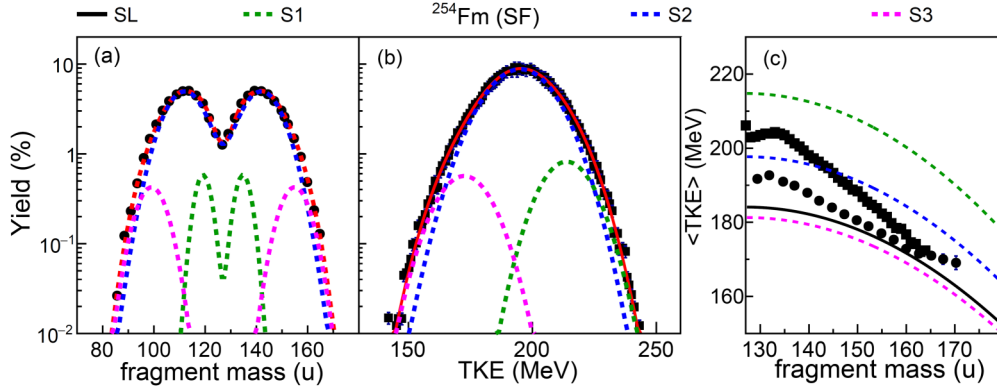


FIG. 2. 1D fitting to the SF (a) MD [52], (b) TKED [29], and (c) $\langle \text{TKE} \rangle$'s [29,52] of the ^{254}Fm nucleus. The solid black circles are from Ref. [52], and the solid black squares are from Ref. [29]. Different Gaussians representing different fission modes are shown by different colors which are listed in the top. The total fits are represented by the continuous orange curves.

heavy prefragment with nucleonic composition that is as close as possible to doubly-magic ^{132}Sn [48]. The predominant S2 mode comes around $M_H \approx 138\text{--}143$ and is due to the deformed shell closure at $N \approx 88$ [50]. With the change in mass of the fissioning nucleus, these peak positions of the heavy fragments, have been found to be stable [15]. The S3 and SA modes are the results of the shell closures at $N \approx 50$ [51] and $Z \approx 28$ with corresponding light fragment mass numbers $M_L \approx 84$ and $M_L \approx 60\text{--}70$, respectively.

Before analyzing the MDs and M-TKEDs of $^{16}\text{O} + ^{238}\text{U}$, the effect of quantum shells on the fission from the ground state, i.e., SF of ^{254}Fm , should be investigated, as shell effects are expected to be the most pronounced at the lowest E^* .

A. Spontaneous fission of ^{254}Fm

The shell effects that might influence the MDs at the higher E^* 's relevant to the reaction $^{16}\text{O} + ^{238}\text{U}$ populating the CN ^{254}Fm can be probed by fitting the SF of the same nucleus ^{254}Fm . The data were taken from the literature [29,52]. The MD data were fitted with the following function [15]:

$$Y(M) = \sum_i \frac{w_i}{\sqrt{2\pi\sigma_i^2}} \times \left[\exp\left(-\frac{(M - \langle M_i \rangle)^2}{2\sigma_i^2}\right) + \exp\left(-\frac{(M - M_{CN} + \langle M_i \rangle)^2}{2\sigma_i^2}\right) \right], \quad (2)$$

where w_i and σ_i are the weights and the widths of the Gaussians centered at $\langle M_i \rangle$'s, corresponding to different fission modes. M_{CN} is the mass of the fissioning nucleus. Four modes (SL, S1, S2, S3) were necessary to fit the data with good accuracy. The SL mode is presented by continuous black lines whereas S1, S2, and S3 modes are shown by dashed green, blue, and magenta lines. The continuous red lines represent the total fits. The mean mass of the SL mode and the width of the S1 mode were fixed at $\frac{M_{CN}}{2}$ and 3.0 u, respectively, in order to avoid nonphysical convergence.

The total kinetic energy (TKE) is also an important observed quantity in nuclear fission, from which the information about the scission configuration can be obtained. As the M-

TKED of SF of ^{254}Fm was not available, the TKED data were fitted separately with the following function [15]:

$$Y(\text{TKE}) = \sum_i h_i \times \left(\frac{200}{\text{TKE}} \right)^2 \times \exp\left(\frac{2(d_{\max,i} - d_{\min,i})}{d_{\text{dec},i}} - \frac{L_i}{d_{\text{dec},i}} - \frac{(d_{\max,i} - d_{\min,i})^2}{L_i d_{\text{dec},i}} \right), \quad (3)$$

where

$$L_i = d - d_{\min,i} = \frac{Z_L Z_H e^2}{\text{TKE}} - d_{\min,i} \approx \frac{\langle M_i \rangle (M_{CN} - \langle M_i \rangle) \left(\frac{Z_{CN}}{M_{CN}} \right)^2 e^2}{\text{TKE}} - d_{\min,i}. \quad (4)$$

Here h_i is the height of the distribution. The maximum TKE is governed by a cutoff due to the Q value of the reaction. The TKED is better represented by a skewed Gaussian distribution. The parameter $d_{\max,i}$ gives distance between the fragment charges at the maximum of the yield distribution, whereas $d_{\min,i}$ is the minimum distance between the fragment charge centers corresponding to an upper limit of the TKE, and the parameter $d_{\text{dec},i}$ describes the exponential decrease of the yield with increasing d (the approximated distance between the two fragment charge centers). $Z_L (M_L)$, $Z_H (M_H)$, $Z_{CN} (M_{CN})$ are the charges (masses) of the light and heavy fragments and CN, respectively. As charges are not measured, one can assume an unchanged charge density, i.e., $Z_L/M_L \approx Z_H/M_H \approx Z_{CN}/M_{CN}$ [53]. The modes present in the MD were accommodated in the TKE fit with the $\langle M_i \rangle$ fixed at the values obtained from the fit to the MD of SF.

The results of the fits are shown in Fig. 2 and the fit parameters are presented in Table I. The S1, S2, and S3 modes are peaking at mean masses 134.80, 141.95, and 154.92, respectively, as expected. The observed differences in the $\langle \text{TKE} \rangle$'s of these modes actually reflect the differences in the charge-center distances between the two fragments at scission

TABLE I. Results of the 1D fitting of the MD and TKED of the SF of ^{254}Fm [29,52]. The distributions were fitted separately (see text). The reduced chi squared ($\tilde{\chi}^2$) of both the fits are given along with the relative yield (Y), average heavy-fragment mass number ($\langle M_H \rangle$), mass width (σ_m), $\langle \text{TKE} \rangle$, and width of the TKED (σ_{TKE}) of the fitted fission modes. Values labeled \dagger were kept fixed during the fitting. The $\langle M_H \rangle$, σ_m , $\langle \text{TKE} \rangle$, and σ_{TKE} values of the fission modes of SF of ^{252}Cf reported by Brosa *et al.* [15] are also given in the last four columns, respectively.

$\tilde{\chi}^2$	Mode	Y (%)	$\langle M_H \rangle$ (u)	σ_m (u)	$\langle \text{TKE} \rangle$ (MeV)	σ_{TKE} (MeV)	$\langle M_H \rangle^{252\text{Cf}}$ (u) [15]	$\sigma_m^{252\text{Cf}}$ (u) [15]	$\langle \text{TKE} \rangle^{252\text{Cf}}$ (MeV) [15]	$\sigma_{\text{TKE}}^{252\text{Cf}}$ (MeV) [15]
0.64 (mass fit)	SL	1.03e-06	127.0 \dagger	8.69 \pm 3.55			127.0	11.6	180.0	7.7
1.46 (TKE fit)		0.05			184.11 \pm 23.67	7.87 \pm 16.73				
(mass fit)	S1	4.28	134.80 \pm 1.94	3.0 \dagger			135.0	3.2	200.0	7.4
(TKE fit)		6.41	134.80 \dagger		213.95 \pm 2.53	9.42 \pm 1.79				
(mass fit)	S2	90.06	141.95 \pm 1.37	7.39 \pm 0.80			143.0	5.0	188.0	8.3
(TKE fit)		88.96	141.95 \dagger		194.96 \pm 0.88	12.16 \pm 0.62				
(mass fit)	S3	5.67	154.92 \pm 4.79	5.43 \pm 1.48			149.0	7.1	176.0	9.5
(TKE fit)		4.58	154.92 \dagger		172.53 \pm 3.08	9.69 \pm 2.18				

for these modes. The SL mode is characterised by $\langle \text{TKE} \rangle$ less than that of S1 or S2, which can be understood by a strong deformation of both fission fragments at the scission configuration. The large error in the $\langle \text{TKE} \rangle$ of the SL mode is due to its very low intensity. This is in agreement with the less/non-presence of the symmetric mode in SF of ^{254}No reported in Ref. [13]. The asymmetric modes S1 and S2 show higher $\langle \text{TKE} \rangle$ [15,47,51,54], for having one spherical heavy fragment and a deformed light fragment in the case of S1 mode and for two moderately deformed fragments in the case of S2 mode at the scission configuration. The values of the $\langle \text{TKE} \rangle$ of SL, S1, S2, and S3 modes agree with the values obtained from the multimodal analysis of the SF of ^{252}Cf [15] (see Table I).

B. One-dimensional fitting of MD of $^{16}\text{O} + ^{238}\text{U}$

The 1D MDs of the reaction under investigation were fitted with Eq. (2). Here, another SA mode was necessary to fit the data properly (dashed orange curves in Fig. 3). This mode can be explained by the influence of $Z = 28$ shell closure. The expected LDM mass width [55] served as the initial parameter for the width of the SL mode. Then the width was fixed at a value where its contribution is maximized and the data are reasonably fitted as well. The idea of maximizing the SL mode is supported by the expected major contribution of the same at such high excitation energies. The uncertainty related to the calculated width of this mode will be discussed in Sec. V. The width of the S1 mode was fixed at 3.0 u. One thing to notice here is that the mean mass of the heavy fragment corresponding to the S3 mode comes out to be 163.61 ± 1.46 after fitting the MD at 45 MeV, whereas, from the fit to the SF of ^{254}Fm , it was found to be 154.92 ± 4.79 . This seems to be produced by the $N \approx 100$ deformed neutron shell in the heavy fragment [34,51]. The considerable shifting of the average mass in the heavy fragment ($\langle M_H \rangle$) of the S3 channel from 148.8 to 158.6 was also observed earlier for fissioning nuclei going from ^{233}Pa to ^{245}Bk [56]. The broadening of the MDs of the standard channels in comparison to the SF distributions is due to the additional E^* 's.

It is well established that with increasing E^* the asymmetric modes fade out due to the disappearance of shell effects, making the decay multimodal to unimodal. Between two main asymmetric modes, at first the S1 mode disappears, followed by S2. The asymmetric modes S3 and SA are less intense [56] and are often not considered in multimodal analysis. At very high excitation the symmetric part would only be left and the fission mechanisms would be described solely by the liquid drop model. This is a signature of the fusion-fission process.

Here, at the 45 MeV excitation, the contributions of S1, S3, and SA modes are found to be small: $\approx 0.39\%$, $\approx 3.38\%$, and $\approx 0.05\%$, respectively. And at 56 MeV excitation the contributions of S1 and SA modes had to be fixed at zero, whereas S3 mode shows a contribution of $\approx 2.12\%$ (see Table II). The contributions of S1, S3, SA have decreased by 100%, 37%,

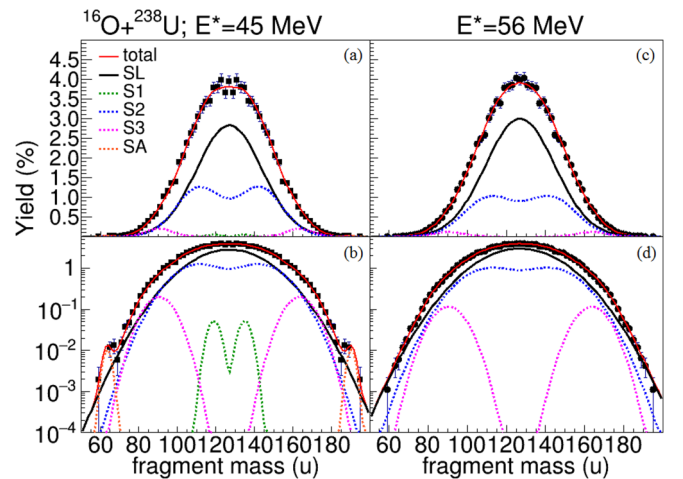


FIG. 3. 1D fitting to the MDs of the reaction $^{16}\text{O} + ^{238}\text{U}$ at two E^* 's: (a), (b) 45 MeV, and (c), (d) 56 MeV. The panels (b) and (d) represent the same results as in panels (a) and (c), respectively, differing only in the use of logarithmic scale in the Y axis for showing fission modes with very low yields clearly. Different Gaussians representing different fission modes are shown by different colors which are listed in panel (a).

TABLE II. Results of the 1D fitting of the MDs of $^{16}\text{O}+^{238}\text{U}$ at two energies. Corresponding E^* 's of the CN are given. Values labeled † were kept fixed during the fitting. The other symbols are same as those described in Table I.

E^* (MeV)	$\tilde{\chi}^2$	Mode	Y (%)	$\langle M_i \rangle$ (u)	σ_m (u)
45	0.82	SL	59.94	127.00 [†]	16.9 [†]
		S1	0.39	135.00 [†]	3.0 [†]
		S2	36.23	143.00 [†]	11.69 ± 0.66
		S3	3.38	163.61 ± 1.46	6.76 ± 0.74
		SA	0.05	63.58 ± 1.03	2.05 ± 0.47
56	0.62	SL	66.27	127.00 [†]	17.6 [†]
		S1	0.0 [†]		
		S2	31.61	143.00 [†]	12.85 ± 0.15
		S3	2.12	163.61 [†]	7.31 ± 0.37
		SA	0.0 [†]		

and 100%, respectively in going ≈ 10 MeV higher in E^* . The rate of decrease of the S1 channel probability is faster than others. Thus, this nucleus is an S1 deceiver [57].

C. Two-dimensional fitting of M-TKEDs of $^{16}\text{O} + ^{238}\text{U}$

It is important to fit both the MD and TKED simultaneously [57] to get a more accurate estimate of the fission modes, as sometimes fitting 1D MD and TKED separately lead to results which do not match. The 2D M-TKEDs were analyzed within the framework of the MM-RNR model [15]

using the following function, which is a combination of Eqs. (2) and (3):

$$Y(M, \text{TKE}) = \sum_i \frac{w_i}{\sqrt{2\pi\sigma_i^2}} \exp\left(-\frac{(M - \langle M_i \rangle)^2}{2\sigma_i^2}\right) \left(\frac{200}{\text{TKE}}\right)^2 \times \exp\left(\frac{2(d_{\max,i} - d_{\min,i})}{d_{\text{dec},i}} - \frac{L_i}{d_{\text{dec},i}} - \frac{(d_{\max,i} - d_{\min,i})^2}{L_i d_{\text{dec},i}}\right), \quad (5)$$

where the symbols represent the same values as described before.

One fission mode in 2D distribution requires six parameters to be fitted. Due to very low yields of very asymmetric and superasymmetric regions, S3 and SA modes could not be accommodated. The mean masses of different fission modes were kept fixed at the values obtained from 1D fitting of MD. The widths of the SL modes were fixed at the values taken from the 1D fitting procedure. As done before, the width of the Gaussian corresponding to S1 mode was fixed at 3.0 u. As prescribed by earlier works [53,58,59], $d_{\min,i}$ were fixed at 11.8 fm in order to avoid nonphysical convergence. This value corresponds to an axis ratio of the deformed nucleus beyond the second minimum [58,60,61]. Variation of $d_{\min,i}$ mainly affects the value of the parameter $d_{\text{dec},i}$, and has no strong effect on the outcome of the fission mode weights [59]. The fits to the data of E^* 's 45 and 56 MeV are shown in Figs. 4 and 5, respectively.

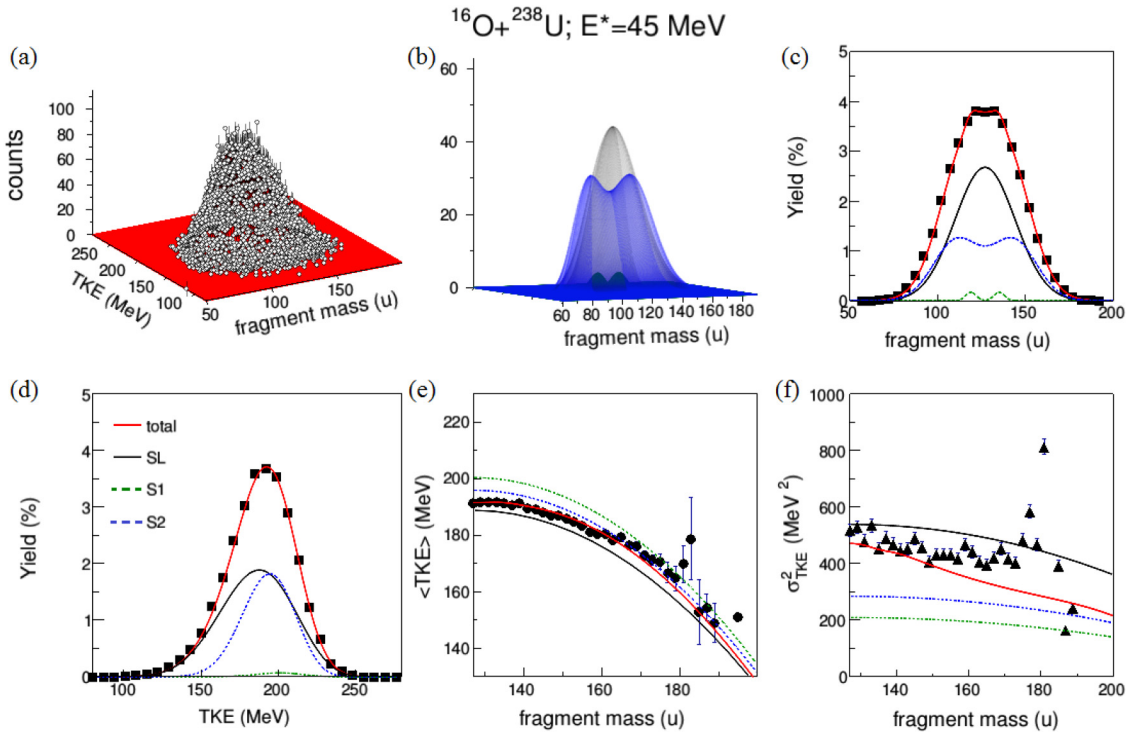
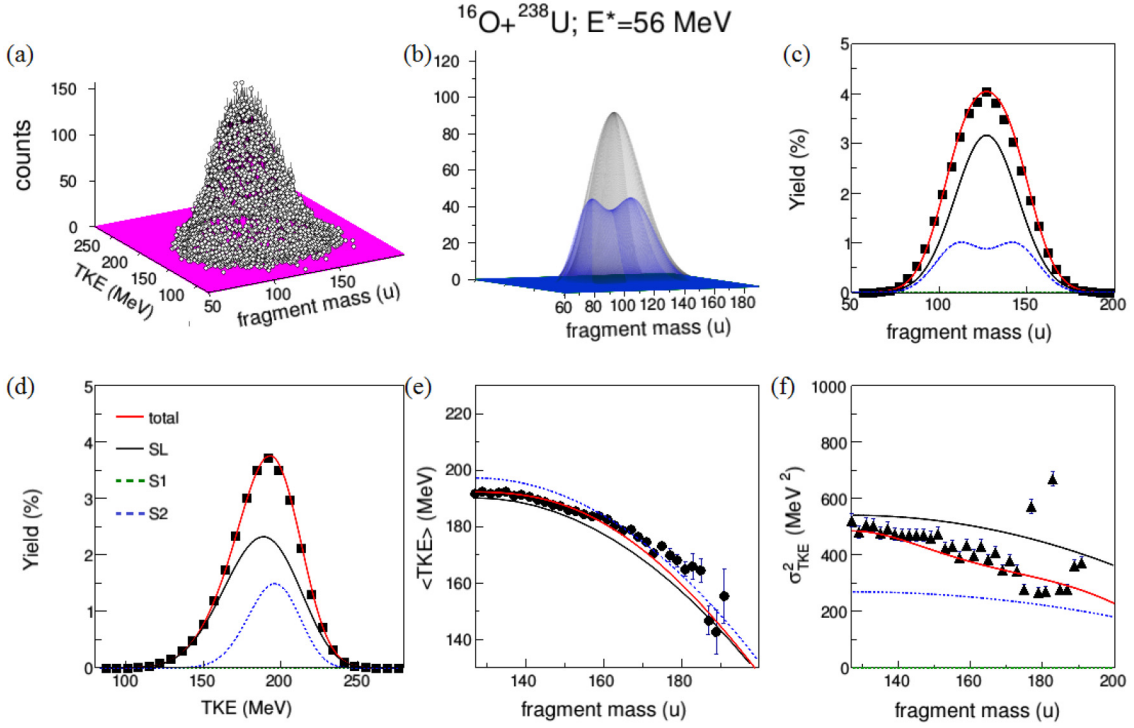


FIG. 4. (a) 2D fit to the M-TKEDs of $^{16}\text{O} + ^{238}\text{U}$ at 45 MeV E^* . (b) The modes which constitute the 2D fit are shown, along with their projections to the (c) X axis (fragment mass) and (d) Y axis (TKE), and the mass dependence of (e) the $\langle \text{TKE} \rangle$ and (f) the σ_{TKE}^2 distributions. The color code is the same as in Fig. 3.

FIG. 5. Same as in Fig. 4 but at 56 MeV E^* .

The increase in the probability of the SL, S1, and S2 modes in comparison to that obtained in the 1D fitting can be attributed to the noninclusion of other asymmetric modes. However, in both the 1D and 2D fits, the probability of the S1 mode is observed to decrease, and that of the SL mode is observed to increase with E^* . The $\langle \text{TKE} \rangle$'s of SL, S1, and S2 modes (≈ 185 , ≈ 200 and ≈ 193 , respectively) are in agreement with the values obtained from the multimodal analysis of the SF of ^{254}Fm in Sec. IV A and of ^{252}Cf [15] (see Tables I and III). Moreover, the $\langle \text{TKE} \rangle$'s and their dispersions σ_{TKE}^2 of the modes show a trend: $\langle \text{TKE} \rangle_{S1} > \langle \text{TKE} \rangle_{S2} > \langle \text{TKE} \rangle_{SL}$ and $\sigma_{\text{TKE},S1}^2 < \sigma_{\text{TKE},S2}^2 < \sigma_{\text{TKE},SL}^2$, respectively. These trends agree with the findings of Refs. [56,62].

Another important thing to observe is that the $\text{TKE}_{\text{Viola}}$ for this reaction (191.3 MeV [44], 195.1 ± 3.2 [63]) matches well with the average TKE of the asymmetric standard S2 mode, $\langle \text{TKE} \rangle_{S2}$ (≈ 193 MeV), not with that of broad symmetric SL mode (≈ 185 MeV).

The ratio of the asymmetric-fission yield (Y_A) to the symmetric-fission yield (Y_S) versus excitation energy (E^*) according to the decompositions of MD and M-TKED of $^{16}\text{O} + ^{238}\text{U}$ (in Figs. 3–5), is presented in Fig. 6. The ratios of $^{18}\text{O} + ^{238}\text{U}$ [64], $^4\text{He} + ^{232}\text{Th}$ [65], and $^{18}\text{O} + ^{208}\text{Pb}$ [66] are also presented for the sake of comparison. It can be seen that the slope of Y_A/Y_S of $^{16}\text{O} + ^{238}\text{U}$ is similar to that of $^{18}\text{O} + ^{208}\text{Pb}$. This almost linear behavior of Y_A/Y_S (in the

TABLE III. Results of 2D fitting of the M-TKEDs of $^{16}\text{O} + ^{238}\text{U}$ at two energies. Corresponding E^* 's of the CN are given. Values labeled † were kept fixed during the fitting. The average kinetic energy release in fission for this reaction obtained from Viola systematics ($\text{TKE}_{\text{Viola}}$) [44,63] is also given. The $\langle M_H \rangle$ and $\langle \text{TKE} \rangle$ values of the fission modes of SF of ^{254}Fm (from Table I) and ^{252}Cf (from Ref. [15]) are also given in the last four columns for the sake of comparison. The other symbols are as described in Table I.

E^* (MeV)	$\tilde{\chi}^2$	Y Mode (%)	$\langle M_i \rangle$ (u)	σ_m (u)	$\langle \text{TKE} \rangle$ (MeV)	$\text{TKE}_{\text{Viola}}$ (MeV)	σ_{TKE} (MeV)	$\langle M_H \rangle_{SF}^{254\text{Fm}}$ (u)	$\langle M_H \rangle_{SF}^{252\text{Cf}}$ (u) [15]	$\langle \text{TKE} \rangle_{SF}^{254\text{Fm}}$ (MeV)	$\langle \text{TKE} \rangle_{SF}^{252\text{Cf}}$ (MeV) [15]	
45	1.01	SL	58.64	127.0 [†]	16.9 [†]	185.3 ± 0.39	191.3	23.2 ± 0.28	127.0	127.0	184.11 ± 23.67	180.0
		S1	1.29	135.0 [†]	3.0 [†]	199.6 ± 1.65	[44]	14.4 ± 1.17	134.80 ± 1.94	135.0	213.95 ± 2.53	200.0
		S2	40.07	143.0 [†]	12.9 ± 0.14	192.8 ± 0.34	195.1 ± 3.2	16.8 ± 0.24	141.95 ± 1.37	143.0	194.96 ± 0.88	188.0
[63]												
56	1.03	SL	69.34	127.0 [†]	17.6 [†]	186.4 ± 0.27		23.3 ± 0.19	127.0	127.0	184.11 ± 23.67	180.0
		S1	0 [†]						134.80 ± 1.94	135.0	213.95 ± 2.53	200.0
		S2	30.66	143.0 [†]	12.9 [†]	194.5 ± 0.28		16.3 ± 0.20	141.95 ± 1.37	143.0	194.96 ± 0.88	188.0

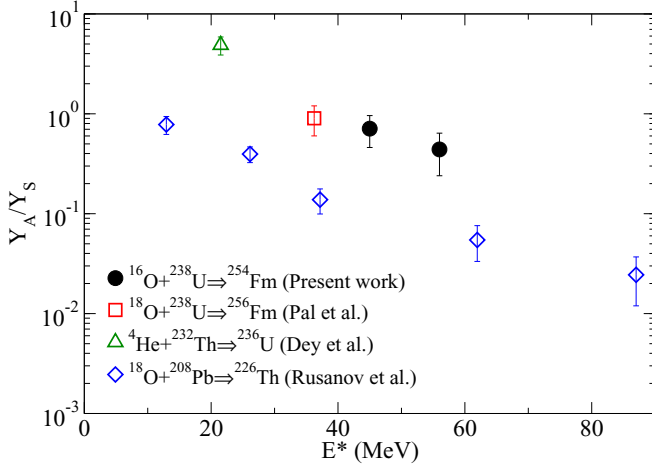


FIG. 6. Ratio of the asymmetric-fission yield Y_A to the symmetric-fission yield Y_S vs excitation energy (E^*) according to the decompositions of MD and M-TKED of $^{16}\text{O} + ^{238}\text{U}$ in Figs. 3–5. The ratios of $^{18}\text{O} + ^{238}\text{U}$ [64], $^4\text{He} + ^{232}\text{Th}$ [65], and $^{18}\text{O} + ^{208}\text{Pb}$ [66] are also presented.

measured energy range) indicates that the shell effects are damped exponentially with increasing excitation energy.

V. COMPARISON OF MASS WIDTHS

The possibility of fast fission in this reaction at both the measured energies is ruled out, as the range of partial waves for fusion at the present energies are well below the angular momentum (see Table IV) at which the fission barrier vanishes ($\ell_{B_f=0}$) [67].

The measured fission fragment mass distribution widths of $^{16}\text{O} + ^{238}\text{U}$ (or $^{238}\text{U} + ^{16}\text{O}$) from this work (solid red circles) and the data taken from literature [1,68–73] are presented in Fig. 7(c). The experimental mass widths for $^{16}\text{O} + ^{238}\text{U}$ from different groups show variation of ≈ 2 –3 u, which might be due to different mass resolutions of different experimental setups. Except for the data from Ref. [71], all other data of $^{16}\text{O} + ^{238}\text{U}$ show mass widths linearly decreasing with decreasing energy (in the c.m. frame) with respect to the Bass barrier [74] ($E_{c.m.}/V_B$). The mass widths were then calculated using the following equation [55] and are shown in Fig. 7(c):

$$\sigma_m^2 = \frac{M_{CN}^2 T_{\text{saddle}}}{16} \left[\left(\frac{d^2V}{d\eta^2} \right)_{\eta=0} \right]^{-1} + \frac{\partial \sigma_m^2}{\partial \langle \ell^2 \rangle} \langle \ell^2 \rangle. \quad (6)$$

TABLE IV. The reaction parameters for $^{16}\text{O} + ^{238}\text{U}$ are presented. The center-of-mass energy ($E_{c.m.}$) is the mean energy in the middle of the target. V_B is the calculated capture barrier of Bass [74]. Also shown are the critical angular momentum $\ell_{\text{crit}}^{\text{fus}}$ for fusion derived from the experimental fusion cross sections [69] assuming the sharp cutoff approximation, the maximum angular momentum $\ell_{\text{max}}^{\text{graz}}$ corresponding to the grazing angle (at the distance of closest approach) [89], and the angular momentum $\ell_{B_f=0}$ for which the fission barrier goes to zero [67]. $Z_P Z_T$, χ_{CN} , χ_{eff} , χ_m , η , and α_{BG} are the charge product, compound nuclear fissility, effective fissility, mean fissility [90], entrance channel mass asymmetry, and Businaro-Gallone critical mass asymmetry [91], respectively. The experimental mass widths (σ_m^{exp}) are also presented.

E_{lab} (MeV)	$E_{c.m.}$ (MeV)	$E_{c.m.}/V_B$	E^* (MeV)	$\ell_{\text{crit}}^{\text{fus}}$ (\hbar)	$\ell_{\text{max}}^{\text{graz}}$ (\hbar)	$\ell_{B_f=0}$ (\hbar)	$Z_P Z_T$	χ_{CN}	χ_{eff}	χ_m	η	α_{BG}	σ_m^{exp} (amu)
89	83.39	0.99	45.06	15	13	60	736	0.842	0.462	0.557	0.874	0.903	19.02 ± 0.059
101	94.64	1.12	56.31	33	38								19.16 ± 0.044

where $\langle \ell^2 \rangle$ are the mean squared angular momenta which were obtained after matching capture cross sections (from CCFULL [75]) with the respective experimental data of $^{16}\text{O} + ^{238}\text{U}$ and $^{238}\text{U} + ^{16}\text{O}$ [1,68,76–78] [Fig. 7(b)]. The Woods-Saxon parametrization of the Akyüz-Winther potential [79] was used for the three ingredients of the nuclear potential used in CCFULL, viz., the depth V_0 , the radius r_0 , and the diffuseness parameter a . Rotational coupling to the target ^{238}U and vibrational coupling to the projectile ^{16}O were taken into account. The r_0 and the a were slightly modified to reproduce the fission data of $^{16}\text{O} + ^{238}\text{U}$ properly. $(\frac{d^2V}{d\eta^2})_{\eta=0}$ is the stiffness of a nucleus for symmetric mass division ($\eta = 0$) and at zero angular momentum, which is taken from the systematics of Ref. [55]. Though the sensitivity of the variance to the angular momentum is much weaker, it was considered, and the term $\frac{\partial \sigma_m^2}{\partial \langle \ell^2 \rangle}$ was taken from the theoretical calculation of Ref. [80]. T_{saddle} is the nuclear temperature at the saddle point.

The calculated mass width values are very sensitive to the used temperature (T). Whether the temperature is calculated considering (1) neutrons (ν) are not emitted before reaching the saddle point ($T = T_{\text{mid}}$), (2) all the neutrons (ν_{pre}) for any nucleus are emitted before reaching the saddle ($T = T_{\text{saddle}}$), (3) only a certain number of neutrons is emitted before reaching the saddle (this depends on the fissility), or (4) mass distribution is formed at the scission point (T_{scission}), can change the calculated mass widths significantly leading to different interpretations. Here, the temperature T was calculated assuming that all the neutrons were emitted before the saddle point (T_{saddle}) [19], using the relation

$$T_{\text{saddle}} = \left(\frac{E_{\text{mid}} - B_f(\ell) - E_n}{a} \right)^{\frac{1}{2}}, \quad (7)$$

where $E_{\text{mid}} = E^* - E_{\text{rot}}^{\text{gs}}(\ell)$ is the excitation energy after subtracting the ℓ -dependent rotational energy of the nucleus in the ground state [$E_{\text{rot}}^{\text{gs}}(\ell)$]. $E^* = E_{c.m.} + Q$ is the initial excitation energy. $E_{c.m.}$ is the energy in the center of mass (c.m.) frame of reference and Q is the Q value for formation of the CN. $B_f(\ell)$ is the ℓ -dependent fission barrier. $B_f(\ell)$ and $E_{\text{rot}}(\ell)$ were calculated by the rotating finite range model (RFRM) of Sierk [67]. The average energy removed by the evaporated neutrons from the CN is denoted by E_n , which was obtained by the following relation:

$$E_n = \langle \nu_{\text{pre}} \rangle \times (B_n + \langle E_{\text{kin}} \rangle), \quad (8)$$

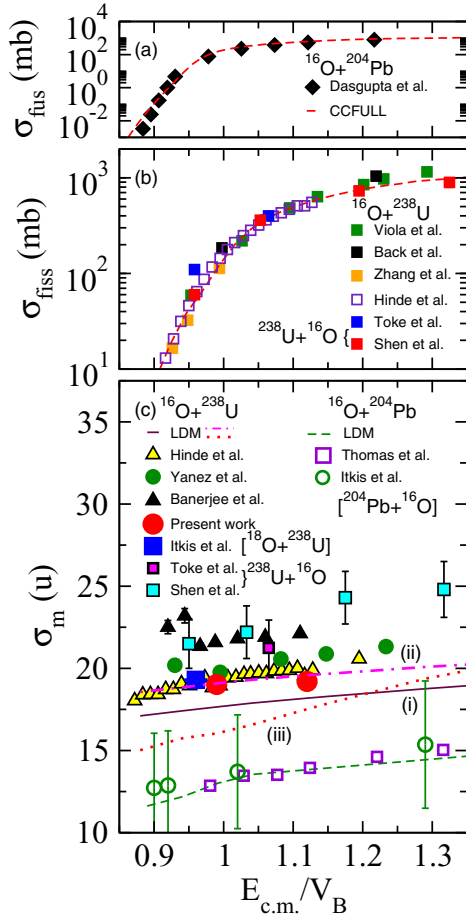


FIG. 7. The comparison of the fusion cross section of $^{16}\text{O} + ^{204}\text{Pb}$ [83] with the calculated capture cross sections from CCFULL [75] is shown in panel (a). (b) Fission cross section data of $^{16}\text{O} + ^{238}\text{U}$ (and $^{238}\text{U} + ^{16}\text{O}$) [1,68,76–78,82] are compared with the calculated capture cross sections, and (c) mass width data of $^{16}\text{O} + ^{238}\text{U}$ (and $^{238}\text{U} + ^{16}\text{O}$) taken from the Refs. [1,68–71] along with the values from the present work (solid red circles) and data of $^{16}\text{O} + ^{204}\text{Pb}$ (and $^{204}\text{Pb} + ^{16}\text{O}$) [84,85] are presented. The LDM mass widths [55,87] for $^{16}\text{O} + ^{238}\text{U}$ and $^{16}\text{O} + ^{204}\text{Pb}$ are also shown (see text). The continuous maroon line and the dot-dashed magenta line are the LDM predictions using the temperature at the saddle point but with level density parameters $a = M_{CN}/8.5$ and $a = M_{CN}/12$, respectively. The dotted red line represents the calculation with scission temperature. The dashed green line for $^{16}\text{O} + ^{204}\text{Pb}$ is the LDM prediction using the temperature at this saddle point with level density parameter $a = M_{CN}/8.5$. V_B is the calculated capture barrier of Bass [74].

where B_n is the neutron binding energy. $\langle \nu_{\text{pre}} \rangle$ were calculated from the systematics of Kozulin *et al.* [55,81]. $\langle E_{\text{kin}} \rangle = 2T_{\text{mid}}$ is the average kinetic energy carried away by the neutrons [19]. $T_{\text{mid}} = \sqrt{E_{\text{mid}}/a}$ is the temperature of nuclei at excitation energy E_{mid} . A level density parameter of $a = M_{CN}/8.5$ [68,82] was used in the calculation.

The reaction $^{16}\text{O} + ^{204}\text{Pb}$, having no transfer induced fission or quasifission, was taken as a reference. The $\langle \ell^2 \rangle$ were obtained matching the measured fusion cross section of $^{16}\text{O} + ^{204}\text{Pb}$ [83] [Fig. 7(a)]. The LDM predictions [dashed

green line in Fig. 7(c)] of the reaction $^{16}\text{O} + ^{204}\text{Pb}$ was first matched with the measured widths of $^{16}\text{O} + ^{204}\text{Pb}$ (and $^{204}\text{Pb} + ^{16}\text{O}$) [84,85]. This provided the reliability of the calculation. Next the mass widths of the reaction $^{16}\text{O} + ^{238}\text{U}$ were calculated. Larger widths for $^{16}\text{O} + ^{238}\text{U}$ in comparison to those of $^{16}\text{O} + ^{204}\text{Pb}$ at the same $E_{c.m.}/V_B$, are expected due to larger $\langle \ell^2 \rangle$ and/or excitations in the former and/or quasifission.

Next, the mass widths of the reaction $^{16}\text{O} + ^{238}\text{U}$ were calculated with the same $a = M_{CN}/8.5$ [continuous maroon line in Fig. 7(c), curve (i)]. The calculation underestimates the data. It can be seen that the present data and the data from Hinde *et al.* [69] of $^{16}\text{O} + ^{238}\text{U}$ coincide and are relatively closer to the calculated values [dot-dashed magenta line in Fig. 7(c), curve (ii)] only when $a = M_{CN}/12$ is used.

Keeping in mind the fact that, for the actinide nuclei, MD is formed at the scission point [68], the mass widths were also calculated with the scission point temperature (T_{scission}) using the following formula:

$$\sigma_m^2 = \frac{1}{k} \sqrt{\frac{8.5E_{\text{scission}}^{\text{eff}}}{M_{CN}}} + \frac{\partial \sigma_m^2}{\partial \langle \ell^2 \rangle} \langle \ell^2 \rangle, \quad (9)$$

where $E_{\text{scission}}^{\text{eff}}$ is the effective E^* at the scission point and is given by

$$E_{\text{scission}}^{\text{eff}} = E^* + Q_{\text{sym}} - \text{TKE}_{\text{Viola}} - E_n - E_{\text{rot}}^{\text{sc}} - E_{\text{def}}, \quad (10)$$

where Q_{sym} is the Q value for symmetric fission of the CN. $E_{\text{rot}}^{\text{sc}}$ is the rotational energy at the scission point obtained following Ref. [55], and E_{def} is the deformation energy at the scission point which was set to 12 MeV, a value used for actinide nucleus fission [82,86]. k is the stiffness parameter for the mass asymmetry degree of freedom and is taken to be 0.0048 MeV/u^2 , which was determined from MDs for the reactions ^{12}C , $^{16}\text{O} + ^{206}\text{Pb}$ [87,88]. The dotted red line in Fig. 7 (c), curve (iii) represents the calculation with scission temperature. Again it fails to reproduce the data. Thus, solely by comparing the experimental MD widths with the calculated ones, no firm conclusion can be made.

VI. DISCUSSION AND CONCLUSIONS

The M-TKEDs of fission fragments of CN ^{254}Fm formed in the reaction $^{16}\text{O} + ^{238}\text{U}$ have been measured at two laboratory energies, $E_{\text{lab}} = 89$ and 101 MeV. The 1D MDs and 2D M-TKEDs of the reaction $^{16}\text{O} + ^{238}\text{U}$ are well described with the aid of the MM-RNR model [15] in this work. The $\langle \text{TKE} \rangle$ and σ_{TKE}^2 are found to follow the trend observed by Brosa *et al.* [15] in a nearby nucleus ^{252}Cf . At an energy close to the Coulomb barrier (89 MeV), evidence of SA mode with a yield of $10^{-2} \%$ is found through 1D fits, but for the same to be observed in the 2D M-TKED may require larger statistics in that region. This signature of SA fission becomes zero at the higher E^* . Probabilities and characteristics of the fission modes are obtained and discussed. It should be mentioned here that these probabilities may vary with the initial condition imposed during the fitting procedure with no or little change in the mean mass and TKE of different fission modes. In the SF-MD and -TKEDs of ^{254}Fm and the distributions of the

reaction $^{16}\text{O} + ^{238}\text{U}$, the high energy symmetric SS mode has not been observed.

The most probable kinetic energy ($\text{TKE}_{\text{Viola}} = 191.3$ MeV) release in fission (in other words the average of the $\langle \text{TKE} \rangle$'s of all the fission modes) is found to be closer to $\langle \text{TKE} \rangle_{S2}$ (≈ 193 MeV), which is similar to the findings of Refs. [31,92]. $\text{TKE}_{\text{Viola}}$ does not match with the $\langle \text{TKE} \rangle$'s of the broad symmetric SL mode (≈ 185 MeV). This may be due to the reduction of $\langle \text{TKE} \rangle$ of the fission fragments with the rising excitation energy, as reported in Refs. [93–97]. We must mention here that the systematic error in measuring energy of ± 5 MeV may add additional uncertainty to the obtained values.

The effects of shells can be present in both the fragmentation of CNF and quasifission. Then certainly a question arises: *How does one distinguish between multimodal fission and quasifission?* One good thing is that, in fission, the effects of shells fade away with increasing E^* . However, even at E^* 's of 50–60 MeV, asymmetric fission modes were found to be present [66,98–100]. The signature of AQF on the MD would be associated with a sharp increase in the yield of asymmetric fission products in the light fragments with masses $60 \leq M_L \leq 90$ (and complementary heavy fragments), as was observed in $^{48}\text{Ca} + ^{168}\text{Er}$, ^{208}Pb , $^{36}\text{S} + ^{238}\text{U}$, and $^{26}\text{Mg} + ^{248}\text{Cm}$ [25,101]. The fission fragment angular distribution for such a “shoulder” showed a pronounced forward-backward asymmetry, which is one of the distinctive features of the quasifission process [102]. Such a prominent, wide asymmetric shoulder is absent in the present data.

Slightly higher $\langle \text{TKE} \rangle$ in the asymmetric mass region compared to the parabolic dependence expected from the LDM (see Fig. 1) indicates this enhancement to be linked to shell effects. Here confusion may arise about the cohabitation of fission products of SA and S3 modes with the AQF wing in the same mass window: the $60 \leq M_L \leq 90$ (and complementary heavy fragments) region. Both of these [(SA+S3) and AQF] disappear toward higher E^* without much change in their respective $\langle M_H \rangle$ values [103]. *How does one distinguish between the AQF shoulder and very asymmetric fission?* Although mass-angle distribution (MAD) [11] and neutron multiplicity (NM) [71] measurements have disproved the presence of AQF in this reaction, it is also true that something of much less intensity cannot be distinguished clearly. If it is coming from AQF at all, then with increasing excitation the peak position and the width of this part would increase and drift toward more symmetric masses, respectively [104]. Further precise measurements at lower and higher excitations can resolve this. In reactions with a uranium target, the AQF peak shifts towards more asymmetric masses with decreasing entrance channel mass asymmetry (η) in the MD. This trend was found to be similar for reactions populating the

same heavy CN [105] also. In contrast to that, in multimodal fission, the position of each mode determined by the nuclear shells is constant for specific CN and only the relative contribution of each mode varies with E^* [15]. Moreover, the similar slope of Y_A/Y_S of $^{16}\text{O} + ^{238}\text{U}$ compared to that of $^{18}\text{O} + ^{208}\text{Pb}$ in Fig. 6 also proves the absence of asymmetric events from AQF in $^{16}\text{O} + ^{238}\text{U}$. Thus, it can be concluded that within the measured energy range of the present reaction, *AQF is absent*.

Assuming unchanged charge density, the heavy fragments of S1 and S2 modes are found to peak at $Z \approx 53$ and $Z \approx 56$, respectively, in this work. This is in agreement with the finding of Böckstiegel *et al.* [106], who found those values stable at $Z \approx 53$ and $Z \approx 55$, respectively, after systematically investigating the characteristics of multimodal fission of 15 nuclei around ^{226}Th .

The fission fragment MD widths show a linear dependence with the measured energies. The anomalous FFAA reported earlier for this reaction [69] in comparison to the LDM predictions, and the usual, linear behavior of fragment MD width, at below barrier energies can be explained by simultaneously considering that the change in the distribution of the orientation of the nuclear symmetry axis relative to the total angular momentum at the saddle point does not seem to affect the mass split, as was concluded in Ref. [70].

Recently, it was shown [9,13] that MD spectra are sensitive to the presence of SQF. Since SQF should occur before any neutron evaporation, unlike fusion-fission, it is therefore expected to occur at a higher E^* , equivalent to that for first-chance CNF. Shell effects in the MD spectra should be more attenuated for SQF than for (multichance) CNF. The presence of SQF is expected to attenuate structure in the MD resulting from shell effects in the nascent fragments, rapidly. Very recently Simenel *et al.* [107] found that a few fission modes can be replaced by quasifission, having been influenced by similar proton/neutron shell closures. Having done a quantitative analysis of fission multimodes, and with the knowledge of their corresponding mean masses, widths, and TKE positions, further work is necessary to look for the interplay among the fission multimodes and quasifission and to distinguish SQF and find a connection with the anomalous sub-barrier FFAA of such reactions.

ACKNOWLEDGMENTS

This work was supported by a program of the Ministry of Energy of the Republic of Kazakhstan (Grant No. BR09158499). We thank the FLNR accelerator team for the quality of beam and nice operation of the cyclotron throughout the experiment. The support of the directorate of the FLNR, JINR is greatly acknowledged.

[1] J. Töke, R. Bock, G. X. Dai, A. Gobbi, S. Gralla, K. D. Hildenbrand, J. Kuzminski, W. F. J. Müller, A. Olmi, H. Stelzer, B. B. Back, and S. Bjørnholm, *Nucl. Phys. A* **440**, 327 (1985); J. Töke, R. Bock, Dai Guang-xi, A. Gobbi, S. Gralla, K. D. Hildenbrand, J. Kuzminski, W. F. J. Müller, A. Olmi,

W. Reisdorf, S. Bjørnholm, and B. B. Back, *Phys. Lett. B* **142**, 258 (1984).

[2] B. Borderie, M. Berlinger, D. Gardés, F. Hanappe, L. Nowicki, J. Péter, B. Tamain, S. Agarwal, J. Girard, C. Gégouire, J. Matuszek, and C. Ngô, *Z. Phys. A* **299**, 263 (1981).

- [3] N. Bohr, *Nature (London)* **137**, 344 (1936).
- [4] S. N. Ghoshal, *Phys. Rev.* **80**, 939 (1950).
- [5] L. Corradi, A. M. Stefanini, C. J. Lin, S. Beghini, G. Montagnoli, F. Scarlassara, G. Pollarolo, and A. Winther, *Phys. Rev. C* **59**, 261 (1999).
- [6] C. Li, J. Tian, and F.-S. Zhang, *Phys. Lett. B* **809**, 135697 (2020).
- [7] E. M. Kozulin, G. N. Knyazheva, I. M. Itkis, M. G. Itkis, A. A. Bogachev, L. Krupa, T. A. Loktev, S. V. Smirnov, V. I. Zagrebaev, J. Äystö, W. H. Trzaska, V. A. Rubchenya, E. Vardaci, A. M. Stefanini, M. Cinausero, L. Corradi, E. Fioretto, P. Mason, G. F. Prete, R. Silvestri, S. Beghini *et al.*, *Phys. Lett. B* **686**, 227 (2010).
- [8] D. J. Hinde, R. du Rietz, M. Dasgupta, R. G. Thomas, and L. R. Gasques, *Phys. Rev. Lett.* **101**, 092701 (2008).
- [9] J. Khuyagbaatar, D. J. Hinde, I. P. Carter, M. Dasgupta, Ch. E. Düllmann, M. Evers, D. H. Luong, R. du Rietz, A. Wakhle, E. Williams, and A. Yakushev, *Phys. Rev. C* **91**, 054608 (2015).
- [10] Y. Aritomo and M. Ohta, *Nucl. Phys. A* **753**, 152 (2005).
- [11] R. du Rietz, E. Williams, D. J. Hinde, M. Dasgupta, M. Evers, C. J. Lin, D. H. Luong, C. Simenel, and A. Wakhle, *Phys. Rev. C* **88**, 054618 (2013).
- [12] I. Halpern and V. M. Strutinsky, in *Proceedings of the 2nd United Nations International Conference on the Peaceful Uses of Atomic Energy, Geneva, 1–13 September 1958*, Vol. 15, Physics in Nuclear Energy (United Nations, Geneva, 1958), p. 408.
- [13] T. Banerjee, D. J. Hinde, D. Y. Jeung, K. Banerjee, M. Dasgupta, A. C. Berriman, L. T. Bezzina, H. M. Albers, Ch. E. Düllmann, J. Khuyagbaatar, B. Kindler, B. Lommel, E. C. Simpson, C. Sengupta, B. M. A. Swinton-Bland, T. Tanaka, A. Yakushev, K. Eberhardt, C. Mokry, J. Runke *et al.*, *Phys. Rev. C* **102**, 024603 (2020).
- [14] G. G. Adamian, N. V. Antonenko, W. Scheid, and V. V. Volkov, *Nucl. Phys. A* **627**, 361 (1997).
- [15] U. Brosa, S. Grossmann, and A. Müller, *Phys. Rep.* **197**, 167 (1990).
- [16] H. C. Britt, H. E. Wegner, and J. C. Gursky, *Phys. Rev.* **129**, 2239 (1963).
- [17] E. Konecky, H. J. Specht, and J. Weber, *Phys. Lett. B* **45**, 329 (1973).
- [18] T. Ohtsuki, H. Nakahara, and Y. Nagame, *Phys. Rev. C* **48**, 1667 (1993).
- [19] I. V. Pokrovsky, L. Calabretta, M. G. Itkis, N. A. Kondratiev, E. M. Kozulin, C. Maiolino, E. V. Prokhorova, A. Ya. Rusanov, and S. P. Tretyakova, *Phys. Rev. C* **60**, 041304(R) (1999).
- [20] K.-H. Schmidt, S. Steinhäuser, C. Böeckstiegel, A. Grewe, A. Heinz, A. R. Junghans, J. Benlliure, H.-G. Clerc, M. de Jong, J. Müller, M. Pfützner, and B. Voss, *Nucl. Phys. A* **665**, 221 (2000).
- [21] P. Siegler, F.-J. Hamsch, S. Oberstedt, and J. P. Theobald, *Nucl. Phys. A* **594**, 45 (1995).
- [22] S. Oberstedt, F.-J. Hamsch, and F. Vivès, *Nucl. Phys. A* **644**, 289 (1998).
- [23] M. G. Itkis, J. Äystö, S. Beghini, A. A. Bogachev, L. Corradi, O. Dorvaux, A. Gadea, G. Giardina, F. Hanappe, I. M. Itkis, M. Jandel, J. Kliman, S. V. Khlebnikov, G. N. Kniajeva, N. A. Kondratiev, E. M. Kozulin, L. Krupa, A. Latina, T. Materna, G. Montagnoli, Yu. Ts. Oganessian *et al.*, *Nucl. Phys. A* **734**, 136 (2004).
- [24] I. V. Pokrovsky, M. G. Itkis, J. M. Itkis, N. A. Kondratiev, E. M. Kozulin, E. V. Prokhorova, V. S. Salamatin, V. V. Pashkevich, S. I. Mulgin, A. Ya. Rusanov, S. V. Zhdanov, G. G. Chubarian, B. J. Hurst, R. P. Schmitt, C. Agodi, G. Bellia, L. Calabretta, K. Lukashin, C. Maiolino, A. Kelic, G. Rudolf *et al.*, *Phys. Rev. C* **62**, 014615 (2000).
- [25] E. V. Prokhorova, A. A. Bogachev, M. G. Itkis, I. M. Itkis, G. N. Knyazheva, N. A. Kondratiev, E. M. Kozulin, L. Krupa, Yu. Ts. Oganessian, I. V. Pokrovsky, V. V. Pashkevich, and A. Ya. Rusanov, *Nucl. Phys. A* **802**, 45 (2008).
- [26] J. P. Balagna, G. P. Ford, D. C. Hoffman, and J. D. Knight, *Phys. Rev. Lett.* **26**, 145 (1971).
- [27] R. M. Harbour, K. W. MacMurdo, D. E. Troutner, and M. V. Hoehn, *Phys. Rev. C* **8**, 1488 (1973).
- [28] R. C. Ragain, E. K. Hulet, R. W. Loughheed, and J. Wild, *Phys. Rev. C* **9**, 399 (1974).
- [29] J. E. Gindler, K. F. Flynn, L. E. Glendenin, and R. K. Sjöblom, *Phys. Rev. C* **16**, 1483 (1977).
- [30] P. Möller, D. G. Madland, A. J. Sierk, and A. Iwamoto, *Nature (London)* **409**, 785 (2001).
- [31] M. D. Usang, F. A. Ivanyuk, C. Ishizuka, and S. Chiba, *Sci. Rep.* **9**, 1525 (2019).
- [32] V. V. Pashkevich, *Nucl. Phys. A* **169**, 275 (1971).
- [33] M. G. Mustafa, U. Mosel, and H. W. Schmitt, *Phys. Rev. C* **7**, 1518 (1973).
- [34] G. Barreau, A. Sicre, F. Caïtucoli, M. Asghar, T. P. Doan, B. Leroux, G. Martinez, and T. Benfoughal, *Nucl. Phys. A* **432**, 411 (1985).
- [35] M. G. Itkis, V. N. Okolovich, A. Ya. Russanov, and G. N. Smirenkin, *Z. Phys. A* **320**, 433 (1985).
- [36] C. Budtz-Jørgensen and H.-H. Knitter, *Nucl. Phys. A* **490**, 307 (1988).
- [37] M. Huhta, P. Dendooven, A. Honkanen, A. Jokinen, G. Lhersonneau, M. Oinonen, H. Penttilä, K. Peräjärvi, V. A. Rubchenya, and J. Äystö, *Phys. Lett. B* **405**, 230 (1997).
- [38] G. Knyazheva, S. N. Dmitriev, M. G. Itkis, I. M. Itkis, E. M. Kozulin, T. Loktev, and Yu. Ts. Oganessian, Exotic Nuclei: EXON-2012, in *Proceedings of the International Symposium*, edited by Y. E. Penionzhkevich and Y. G. Sobolev (World Scientific, Singapore, 2013), p. 167.
- [39] K. B. Gikal, E. M. Kozulin, I. M. Itkis, M. G. Itkis, G. N. Knyazheva, K. V. Novikov, and A. N. Pan, *Bull. Russ. Acad. Sci. Phys.* **82**, 716 (2018).
- [40] H. J. Lustig, J. A. Maruhn, and W. Greiner, *J. Phys. G: Nucl. Phys.* **6**, L25 (1980).
- [41] E. M. Kozulin, A. A. Bogachev, M. G. Itkis, I. M. Itkis, G. N. Knyazheva, N. A. Kondratiev, L. Krupa, I. V. Pokrovsky, and E. V. Prokhorova, *Instrum. Exp. Tech.* **51**, 44 (2008).
- [42] I. M. Itkis, A. A. Bogachev, A. Yu. Chizhov, D. M. Gorodisskiy, M. G. Itkis, G. N. Knyazheva, N. A. Kondratiev, E. M. Kozulin, L. Krupa, S. I. Mulgin, I. V. Pokrovsky, E. V. Prokhorova, A. Ya. Rusanov, V. M. Voskressenski, and S. V. Zhdanov, *Phys. Lett. B* **640**, 23 (2006).
- [43] J. R. Nix and W. J. Swiatecki, *Nucl. Phys.* **71**, 1 (1965).
- [44] V. E. Viola, Jr., *Nucl. Data Sheets* **A1**, 391 (1965).
- [45] J. van Aarle, W. Westmeier, R. A. Esterlund, and P. Patzelt, *Nucl. Phys. A* **578**, 77 (1994).
- [46] Z. Büyükmumcu and M. Kildir, *Phys. Rev. C* **74**, 054613 (2006).
- [47] T. Ohsawa, T. Horiguchi, and H. Hayashi, *Nucl. Phys. A* **653**, 17 (1999); T. Ohsawa, *ibid.* **665**, 3 (2000).

- [48] S. I. Mulgin, S. V. Zhdanov, N. A. Kondratiev, K. V. Kovalchuk, and A. Ya. Rusanov, *Nucl. Phys. A* **824**, 1 (2009).
- [49] D. Rochman, I. Tsekhanovich, F. Gönnerwein, V. Sokolov, F. Storrer, G. Simpson, and O. Serot, *Nucl. Phys. A* **735**, 3 (2004).
- [50] B. D. Wilkins, E. P. Steinberg, and R. R. Chasman, *Phys. Rev. C* **14**, 1832 (1976).
- [51] P. Schillebeeckx, C. Wagemans, A. J. Deruytter, and R. Barthélémy, *Nucl. Phys. A* **545**, 623 (1992).
- [52] R. Brandt, S. G. Thompson, R. C. Gatti, and L. Phillips, *Phys. Rev.* **131**, 2617 (1963).
- [53] A. Al-Adili, F.-J. Hamsch, S. Pomp, S. Oberstedt, and M. Vidali, *Phys. Rev. C* **93**, 034603 (2016).
- [54] K.-H. Schmidt and B. Jurado, *EPJ Web Conf.* **8**, 03002 (2010).
- [55] M. G. Itkis and A. Ya. Rusanov, *Phys. Part. Nuclei* **29**, 160 (1998).
- [56] S. I. Mulgin, V. N. Okolovich, and S. V. Zhdanova, *Phys. Lett. B* **462**, 29 (1999).
- [57] U. Brosa, H.-H. Knitter, T.-S. Fan, J.-M. Hu, and S. L. Bao, *Phys. Rev. C* **59**, 767 (1999).
- [58] E. Birgersson, A. Oberstedt, S. Oberstedt, and F.-J. Hamsch, *Nucl. Phys. A* **817**, 1 (2009).
- [59] A. Göök, M. Chernykh, C. Eckardt, J. Enders, P. von Neumann-Cosel, A. Oberstedt, S. Oberstedt, and A. Richter, *Nucl. Phys. A* **851**, 1 (2011).
- [60] L. Bonneau, *Phys. Rev. C* **74**, 014301 (2006).
- [61] Y. Miyamoto, Y. Aritomo, S. Tanaka, K. Hirose, and K. Nishio, *Phys. Rev. C* **99**, 051601(R) (2019).
- [62] S. D. Beizin, S. V. Zhdanov, M. G. Itkis, V. N. Okolovich, G. N. Smirenkin, and M. I. Subbotin, *Sov. J. Nucl. Phys.* **53**, 411 (1991).
- [63] V. E. Viola, K. Kwiatkowski, and M. Walker, *Phys. Rev. C* **31**, 1550 (1985).
- [64] A. Pal, S. Santra, P. C. Rout, Ramandeep Gandhi, Abhijit Baishya, T. Santhosh, R. Tripathi, and T. N. Nag, *Phys. Rev. C* **104**, L031602 (2021).
- [65] A. Dey, D. C. Biswas, A. Chakraborty, S. Mukhopadhyay, A. K. Mondal, K. Mandal, B. Mukherjee, R. Chakrabarti, B. N. Joshi, L. A. Kinage, S. Chatterjee, S. Samanta, S. Das, S. Bhattacharya, R. Banik, S. Nandi, Shabir Dar, R. Raut, G. Mukherjee, S. Bhattacharyya, S. S. Ghugre *et al.*, *Phys. Lett. B* **825**, 136848 (2022).
- [66] A. Ya. Rusanov, M. G. Itkis, N. A. Kondratiev, V. V. Pashkevich, I. V. Pokrovsky, V. S. Salamatina, and G. G. Chubarina, *Phys. At. Nucl.* **71**, 956 (2008).
- [67] A. J. Sierk, *Phys. Rev. C* **33**, 2039 (1986).
- [68] W. Q. Shen, J. Albinski, A. Gobbi, S. Gralla, K. D. Hildenbrand, N. Herrmann, J. Kuzminski, W. F. J. Müller, H. Stelzer, J. Töke, B. B. Back, S. Bjørnholm, and S. P. Sørensen, *Phys. Rev. C* **36**, 115 (1987).
- [69] D. J. Hinde, M. Dasgupta, J. R. Leigh, J. C. Mein, C. R. Morton, J. O. Newton, and H. Timmers, *Phys. Rev. C* **53**, 1290 (1996).
- [70] R. Yanez, D. J. Hinde, B. Bouriquet, and D. Duniec, *Phys. Rev. C* **71**, 041602(R) (2005).
- [71] K. Banerjee, T. K. Ghosh, S. Bhattacharya, C. Bhattacharya, S. Kundu, T. K. Rana, G. Mukherjee, J. K. Meena, J. Sadhukhan, S. Pal, P. Bhattacharya, K. S. Golda, P. Sugathan, and R. P. Singh, *Phys. Rev. C* **83**, 024605 (2011).
- [72] Yu. M. Itkis, A. V. Karpov, G. N. Knyazheva, E. M. Kozulin, N. I. Kozulina, K. V. Novikov, K. B. Gikal, I. N. Diatlov, I. V. Pchelintsev, I. V. Vorobiov, A. N. Pan, and P. P. Singh, *Bull. Russ. Acad. Sci. Phys.* **84**, 938 (2020).
- [73] T. Banerjee, E. M. Kozulin, K. B. Gikal, I. M. Itkis, G. N. Knyazheva, N. I. Kozulina, K. V. Novikov, I. N. Diatlov, I. V. Pchelintsev, A. N. Pan, and I. V. Vorobiev, *Phys. Part. Nuclei* **53**, 135 (2022).
- [74] R. Bass, *Nuclear Reactions with Heavy Ions* (Springer, New York, 1980), Chap. 7.4, pp. 318–340.
- [75] K. Hagino, N. Rowley, and A. J. Kruppa, *Comput. Phys. Commun.* **123**, 143 (1999).
- [76] V. E. Viola, Jr. and T. Sikkeland, *Phys. Rev.* **128**, 767 (1962).
- [77] D. J. Hinde, M. Dasgupta, J. R. Leigh, J. P. Lestone, J. C. Mein, C. R. Morton, J. O. Newton, and H. Timmers, *Phys. Rev. Lett.* **74**, 1295 (1995).
- [78] H. Zhang, Z. Liu, J. Xu, X. Qian, Y. Qiao, C. Lin, and K. Xu, *Phys. Rev. C* **49**, 926 (1994).
- [79] R. A. Broglia and A. Winther, *Heavy Ion Reactions* (Benjamin-Cummings, Reading, MA, 1981), Vol. 1.
- [80] G. D. Adeev and V. V. Pashkevich, *Nucl. Phys. A* **502**, 405 (1989).
- [81] E. M. Kozulin, A. Ya. Rusanov, and G. N. Smirenkin, *Yad. Fiz.* **56**, 37 (1993); *Phys. At. Nucl.* **56**, 166 (1993).
- [82] B. B. Back, R. R. Betts, J. E. Gindler, B. D. Wilkins, S. Saini, M. B. Tsang, C. K. Gelbke, W. G. Lynch, M. A. McMahan, and P. A. Baisden, *Phys. Rev. C* **32**, 195 (1985).
- [83] M. Dasgupta, D. J. Hinde, A. Diaz-Torres, B. Bouriquet, C. I. Low, G. J. Milburn, and J. O. Newton, *Phys. Rev. Lett.* **99**, 192701 (2007).
- [84] M. G. Itkis *et al.*, Large-scale collective motion of atomic nuclei, in *Proceedings of the Conference, Brolo, Messina, Italy, 1996*, edited by G. Giardina *et al.* (World Scientific, Singapore 1996), pp. 270–281; JINR Technical Report JINR-E-7-96-414, 1996 (unpublished); in *Tours Symposium on Nuclear Physics III, 2–5 September 1997, Tours, France*, edited by M. Arnould, M. Lewitowicz, Yu. Ts. Oganessian, M. Ohta, H. Utsunomiya, and T. Wada, AIP Conf. Proc. No. 425 (AIP, New York, 1998), p. 189.
- [85] R. G. Thomas, D. J. Hinde, D. Duniec, F. Zenke, M. Dasgupta, M. L. Brown, M. Evers, L. R. Gasques, M. D. Rodriguez, and A. Diaz-Torres, *Phys. Rev. C* **77**, 034610 (2008).
- [86] C. J. Lin, R. du Rietz, D. J. Hinde, M. Dasgupta, R. G. Thomas, M. L. Brown, M. Evers, L. R. Gasques, and M. D. Rodriguez, *Phys. Rev. C* **85**, 014611 (2012).
- [87] B. B. Back, P. B. Fernandez, B. G. Glagola, D. Henderson, S. Kaufman, J. G. Keller, S. J. Sanders, F. Videbæk, T. F. Wang, and B. D. Wilkins, *Phys. Rev. C* **53**, 1734 (1996).
- [88] M. G. Itkis, S. M. Lukyanov, V. N. Okolovich, A. Ya. Rusanov, V. S. Salamatina, and G. G. Chubarina, *Yad. Fiz.* **52**, 23 (1990) [*Sov. J. Nucl. Phys.* **52**, 15 (1990)].
- [89] J. R. Birkelund, J. R. Huizenga, H. Freiesleben, K. L. Wolf, J. P. Unik, and V. E. Viola, Jr., *Phys. Rev. C* **13**, 133 (1976).
- [90] J. P. Blocki, H. Feldmeier, and W. J. Swiatecki, *Nucl. Phys. A* **459**, 145 (1986).
- [91] U. L. Businaro and S. Gallone, *Nuovo Cimento* **5**, 315 (1957).
- [92] T. Ohsawa, *J. Nucl. Radiochem. Sci.* **3**, 93 (2002).
- [93] V. Yu. Denisov and I. Yu. Sedykh, *Phys. Lett. B* **824**, 136814 (2022).
- [94] D. G. Madland, *Nucl. Phys. A* **772**, 113 (2006).
- [95] J. P. Lestone and T. T. Strother, *Nucl. Data Sheets* **118**, 208 (2014).

- [96] R. Yanez, J. King, J. S. Barrett, W. Loveland, N. Fotiades, and H. Y. Lee, *Nucl. Phys. A* **970**, 65 (2018).
- [97] A. Pica, A. T. Chemey, L. Yao, W. Loveland, H. Y. Lee, and S. A. Kuvvin, *Phys. Rev. C* **102**, 064612 (2020).
- [98] I. V. Ryzhov, S. G. Yavshits, G. A. Tutin, N. V. Kovalev, A. V. Saulski, N. A. Kudryashev, M. S. Onegin, L. A. Vaishnena, Yu. A. Gavrikov, O. T. Grudzevich, V. D. Simutkin, S. Pomp, J. Blomgren, M. Österlund, P. Andersson, R. Bevilacqua, J. P. Meulders, and R. Prieels, *Phys. Rev. C* **83**, 054603 (2011).
- [99] R. Leguillon, K. Nishio, K. Hirose, H. Makii, I. Nishinaka, R. Orlandi, K. Tsukada, J. Small-combe, S. Chiba, Y. Aritomo, T. Ohtsuki, R. Tatsuzawa, N. Takaki, N. Tamura, S. Goto, I. Tsekhanovich, C. M. Petrache, and A. N. Andreyev, *Phys. Lett. B* **761**, 125 (2016).
- [100] J. King, R. Yanez, W. Loveland, J. S. Barrett, J. S. Barrett, B. Oscar, N. Fotiades, F. Tovesson, and H. Y. Lee, *Eur. Phys. J. A* **53**, 238 (2017).
- [101] M. G. Itkis, E. Vardaci, I. M. Itkis, G. N. Knyazheva, and E. M. Kozulin, *Nucl. Phys. A* **944**, 204 (2015).
- [102] A. Yu. Chizhov, M. G. Itkis, I. M. Itkis, G. N. Kniajeva, E. M. Kozulin, N. A. Kondratiev, I. V. Pokrovsky, R. N. Sagaidak, V. M. Voskressensky, A. V. Yerebin, L. Corradi, A. Gadea, A. Latina, A. M. Stefanini, S. Szilner, M. Trotta, A. M. Vinodkumar, S. Beghini, G. Montagnoli, F. Scarlassara, A. Ya. Rusanov, F. Hanappe *et al.*, *Phys. Rev. C* **67**, 011603(R) (2003).
- [103] I. M. Itkis, E. M. Kozulin, M. G. Itkis, G. N. Knyazheva, A. A. Bogachev, E. V. Chernysheva, L. Krupa, Yu. Ts. Oganessian, V. I. Zagrebaev, A. Ya. Rusanov, F. Goennenwein, O. Dorvaux, L. Stuttgé, F. Hanappe, E. Vardaci, and E. de Goés Brenand, *Phys. Rev. C* **83**, 064613 (2011).
- [104] G. N. Knyazheva, I. M. Itkis, and E. M. Kozulin, *J. Phys.: Conf. Ser.* **515**, 012009 (2014).
- [105] E. M. Kozulin, M. G. Itkis, and G. N. Knyazheva, *J. Phys.: Conf. Ser.* **282**, 012008 (2011).
- [106] C. Böckstiegel, S. Steinhäuser, K.-H. Schmidt, H.-G. Clerc, A. Grewe, A. Heinz, M. de Jong, A. R. Junghans, J. Müller, and B. Voss, *Nucl. Phys. A* **802**, 12 (2008).
- [107] C. Simenel, P. McGlynn, A. S. Umar, and K. Godbey, *Phys. Lett. B* **822**, 136648 (2021).